1962

Study of the design of reinforcement for prestressed concrete and blocks

Charles Robert Hoffman

Department:

STUDY OF THE DESIGN OF REINFORCEMENT FOR PRESTRESSED CONCRETE END BLOCKS

BY

CHARLES ROBERT HOFFMAN

A

THESIS

submitted to the faculty of the

SCHOOL OF MINES AND METALLURGY OF THE UNIVERSITY OF MISSOURI

in partial fulfillment of the requirements for the

Degree of

MASTER OF SCIENCE IN CIVIL ENGINEERING

Rolla, Missouri

1962

Approved by

John L. Best (advisor) F. L. Ritchey

John B. Scrivner Jr. R. J. Davidson

ABSTRACT

This thesis is an analysis of the transverse tensile stress condition in an end block of a prestressed concrete beam. A stress analysis was made by photoelasticity and compared to the mathematical solutions and experimental solutions performed by others on concrete models. The photoelastic model was made from a piece of Columbia Resin, 39.

Whatever method is chosen to determine the stress condition, there is no exact code that can be established to fit the various type problems which arise.

ACKNOWLEDGMENT

The author desires to express his sincere appreciation to Professor E. W. Carlton, Chairman of the Department of Civil Engineering, for his help and guidance throughout the investigation of this problem.

The author wishes to especially express his sincere appreciation to Associate Professor John L. Best who suggested the problem and who gave constant advice during the preparation of this paper.

The author also wishes to thank Associate Professor John B. Heagler, Jr. for his advice and complete review of this thesis.

TABLE OF CONTENTS

LIST OF FIGURES

STUDY OF THE DESIGN OF REINFORCEMENT FOR PRESTRESSED CONCRETE END BLOCKS

INTRODUCTION

Since the beginning of the twentieth century, concrete has taken its place as one of the most useful and important structural materials. There are many reasons responsible for the growth of concrete construction, several of which are the local availability of a large portion of the material used in concrete, the ability to be formed into any shape, and because it is very pleasing to the eye.

One of the early disadvantages noted in the use of concrete was its inability to resist tensile stresses. As time went along, engineers found by placing steel bars on the tensile side of a flexural member, that the tensile load would be carried solely by the steel bars. This produced a low-cost material capable of carrying compressive stresses and with the addition of a small amount of steel, it has the ability to resist tensile stresses. The concrete on the tensile side of the neutral axis serves two main purposes; it provides a connection between the compressive concrete and the steel and secondly helps resist diagonal tension stresses. The tensile concrete is considered cracked, by design procedures, and therefore cannot resist tension. This concrete below the neutral axis results in useless dead weight with the exception of the ability to resist diagonal tension stresses.

Around 1949 a new concept, in reinforced concrete construction, was introduced into the United States called prestressed concrete.

Although accepted only a few years ago, the idea of prestressing was applied perhaps centuries ago. As an example of the idea of prestressing centuries ago, wooden barrels were made with staves and metal bands around the outside. This produced stress conditions similar to that of a prestressed concrete beam in that the metal bands were placed in tension and the wooden staves were placed in compression.

With the acceptance of the prestressed concrete idea, architects and engineers have designed and built structures never before dreamed of by man. Prestressed concrete goes two steps beyond reinforced concrete. First, all of the concrete on the tensile side of the neutral axis is put under an initial compressive stress of such a magnitude that all design loads which are to be applied to the structure in the future can reduce this stress but will not put the concrete in tension (Figure 1). Secondly the prestress is applied in such a manner that it creates a bending moment of opposite sign to those which will be produced by applied dead and live loads.[1] (Figure 2). In the actual construction of a structure the compressive stresses may be applied in one of three ways; by post-tensioning, by pre-tensioning or by prestressing externally. Post-tensioning is applied to all systems in which the steel is tensioned after the concrete has been cast and matured. Pre-tensioning is a method in which the steel is tensioned before the concrete is cast, the wires being temporarily anchored against rigid supports. The third method, prestressing externally, is similar to post-tensioning in that the steel is not tensioned until after the curing process but differs in design in that the steel is usually tensioned on the exterior surface of the beam.

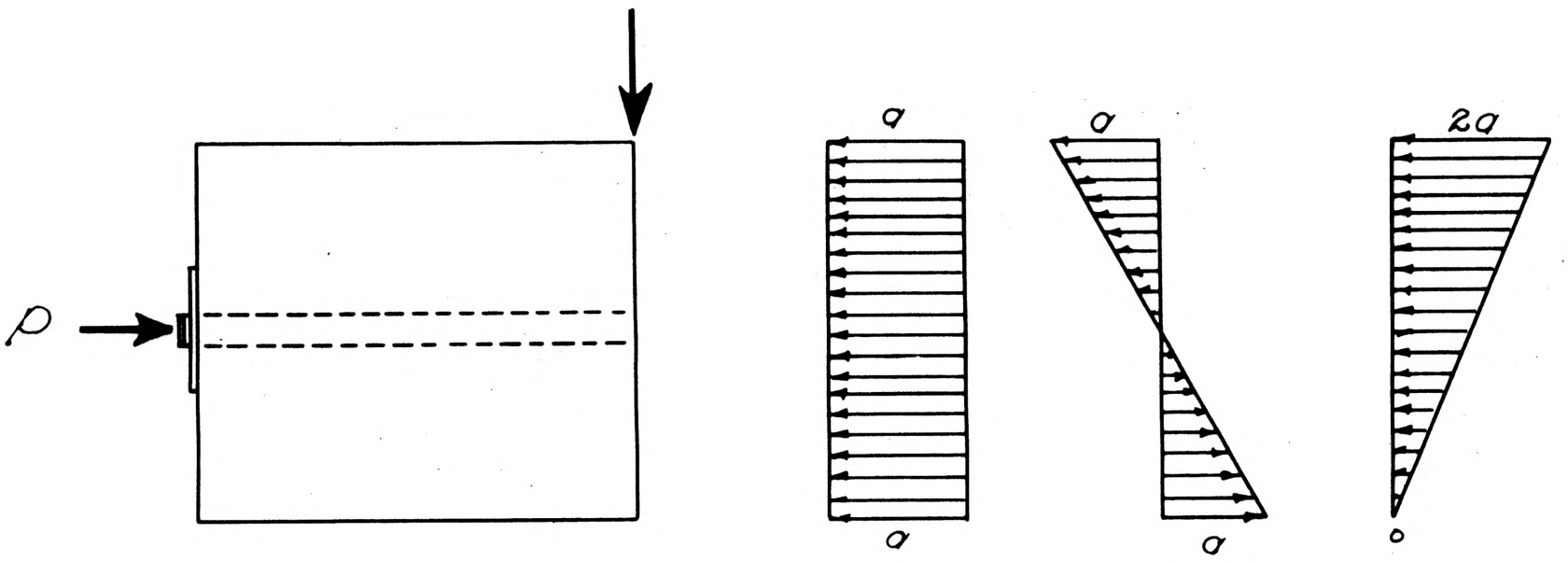

Stress Diagram P/A, Mc/I, and Composite

Figure (1)

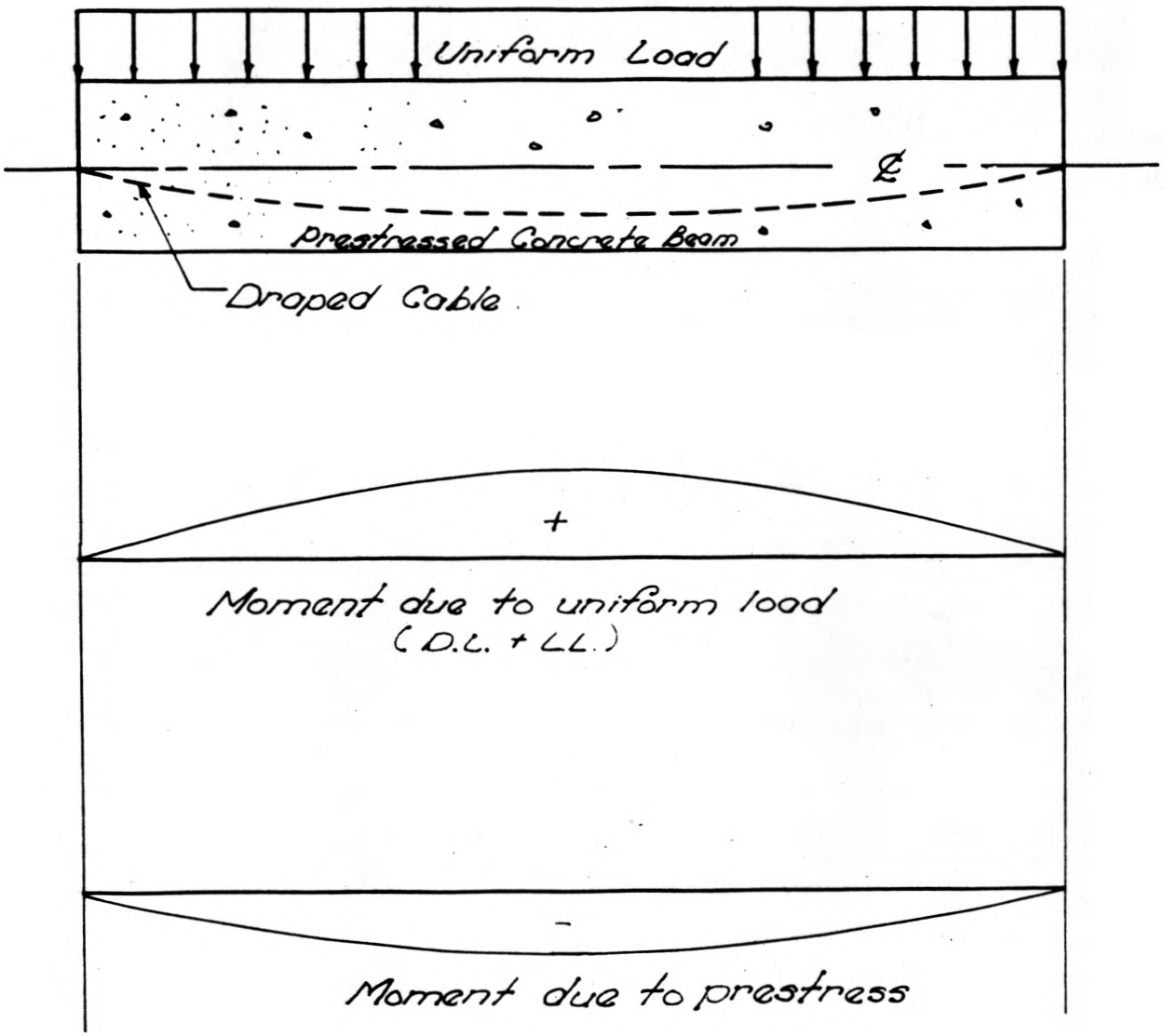

Net effect reduction of moment

Figure (2)

One of the largest demands for prestressed concrete is in the design of beams. Prestressed beams are capable of spanning greater distances and the size required, to carry the same load as the conventional reinforced concrete beam, is much smaller.

One disadvantage noted in working with the prestressed concrete is the highly skilled and technical working crew required to efficiently operate a plant and or project. This results in increased labor costs, but overall savings may offset these costs when compared with other types of construction.

There are many design considerations which engineers have been confronted with in the design of prestressed concrete beams. Some of these design considerations are the initial prestress required in the steel, placement of the prestressing steel and the use of the loading devices now available on the market. These problems have been solved by experimental methods or by mathematical calculations.

There is one very important design consideration remaining to be solved and that is the design of an end block for a prestressed concrete beam. Theend block is that portion at the end of a prestressed beam which surrounds the anchorages of the tendons, (Figure 3). Throughout the length of the end block, prestress is transferred from areas of high stress concentration and distributed throughout the entire beam section. The necessary length of an end block or lead-in zone as it is sometimes referred to, has been found both mathematically and experimentally to be approximately equal to the depth of the beam. As stated in the Tentative Recommendations for Prestressed Concrete, "The size of the end block is usually proportioned by experience."[2]

The determination of the stresses in end blocks is a complex problem, and the mathematical methods available are either extremely lengthy or involve sweeping assumptions. The experimental investigation of actual concrete end blocks has not yet been carried out to any great extent; photo-elastic work is promising, but neither has this reached a stage to be of direct value to the designer.(3)

It is the intention of this author to review all available sources of information and with the use of photoelasticity, check results of transverse tensile stresses as obtained by various authors. Then, using the stress values obtained by the photoelastic methods, determine the amount of reinforcing steel required in the end zone of an example problem.

REVIEW OF LITERATURE

There are always concentrations of forces which must be evaluated or at least approximated, in the design of a post tensioned beam. Whatever process is employed in creating the prestressing forces, whether it be by jacks on external abutments or jacks bearing against the end of a beam, these stresses present problems to the engineer.

The term "lead-in zone" will be applied to the zone of the beam lying between the surface on which the prestress forces act and that section which a linear distribution of stress is first attained. In this lead-in zone, the longitudinal stresses must pass progressively from the discontinuous distribution to the continuous uniform stress condition, (Figure 3). This progression cannot be made without giving rise to transverse stresses and to shear stresses along both horizontal and vertical longitudinal planes.(4)

Guyon and his associate, E. Freyssinet, limited their work on prestressed concrete to the study of straight beams on two supports. The analysis and study of such a simple structure as this gives an idea of the number and complexity of the problems met in prestressed concrete design.(4)

In Guyon's discussion of the stress distribution which exists in the short distance, represented by the lead-in zone, he concludes that the stress distribution can only be solved by the advanced theory of elasticity, which is complicated even for the simplest conditions of loading. In order to simplify the stress distribution, Guyon makes an assumption that the load is uniformly distributed across the width of

the beam, thus, instead of a load concentrated at one point, he assumes a knife edge load extending the entire width of the beam. The problem is then reduced from a three dimensional problem to a two dimensional problem, (Figure 3). As a result of this knife edge load extending the full width of the beam, stress calculations are made on a vertical longitudinal plane ABCD, Figure 3. Zero stress is assumed in the direction of the width of the beam. Similar stress calculations can be made on a horizontal longitudinal plane by assuming a knife edge load acting across the depth of the beam rather than the width. Zero stress is then assumed in the direction of the depth of the beam.(4)

By applying this knife edge load, in experimental studies, shear and transverse stresses were found to exist along vertical and horizontal planes throughout the lead-in zone. Those stresses most critical were along the axis of the applied load. In general the shearing stresses were small with relation to allowable stresses and only the transverse tensile stresses produced strains which were considered to be critical. These stresses were actually computed for the exterior surface. Guyon assumed the same stress distribution existed along a vertical plane through the center line of the beam, in the vicinity of the applied force. As a result of the above assumption, average stresses were computed. This average stress condition would not be the case in actual practice because of the discontinuous load arrangements.

An ideal situation would exist if the load was uniformly distributed across the entire end surface of the beam. This would

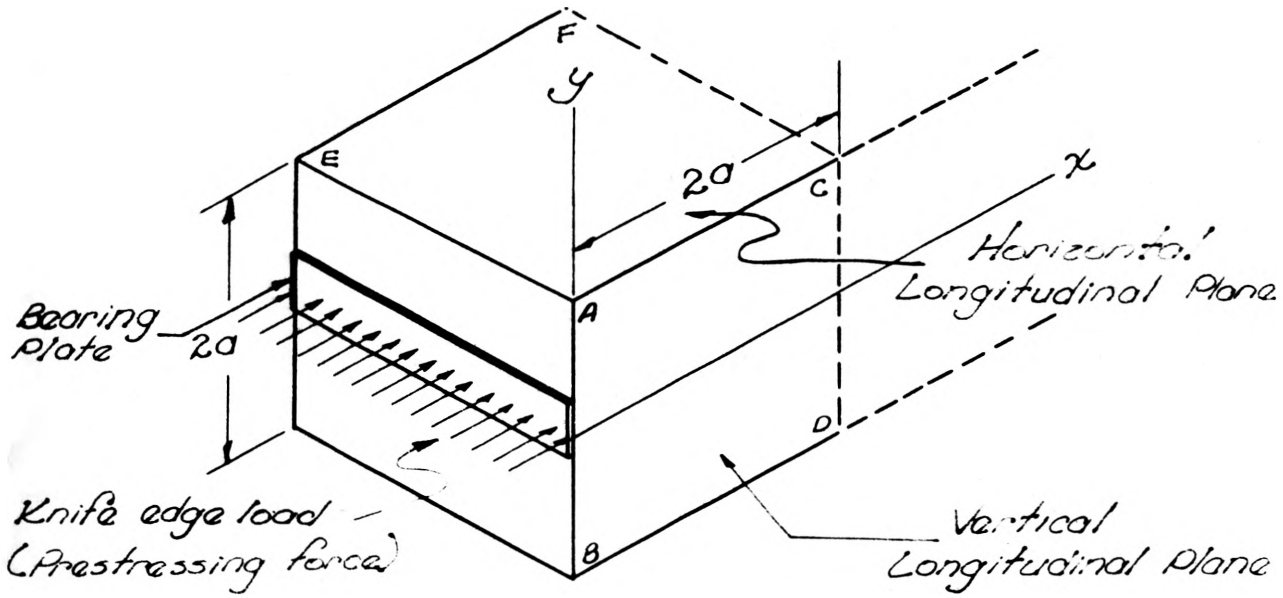

Diagram showing lead-in zone (ABCD)

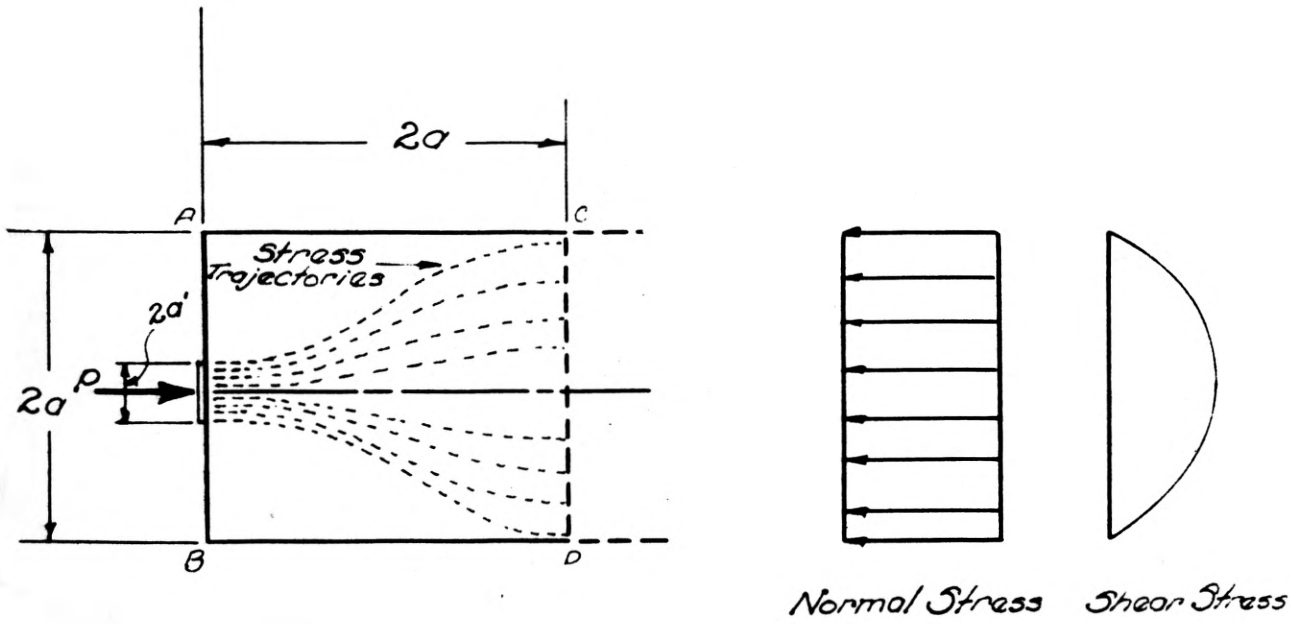

Stress Trajectories used to show discontinuous to continuous stress distribution

Figure (3)

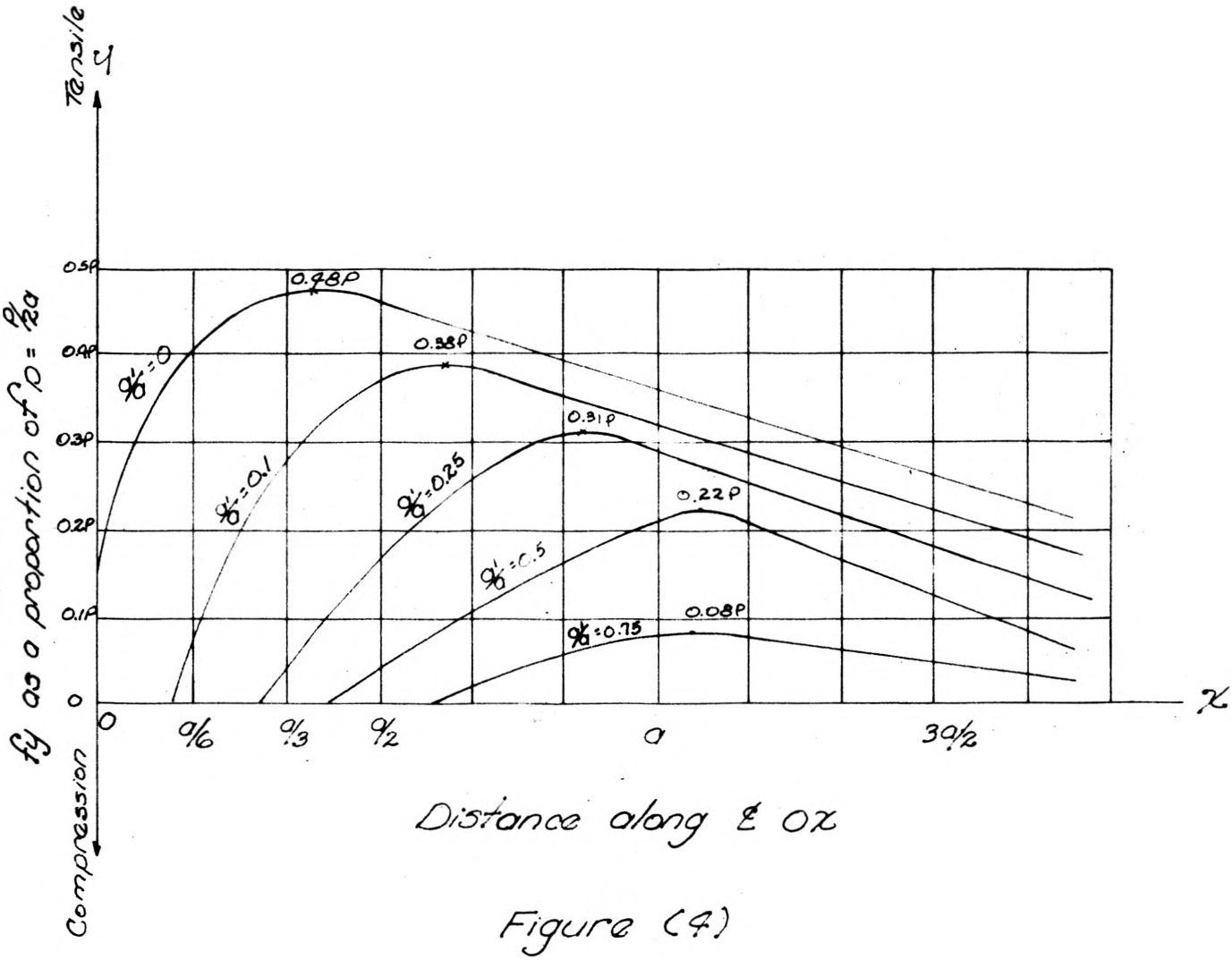

Figure (4)

Y. Guyon, Prestressed Concrete Page 132

Graph of Transverse stress versus distance along ℄ of applied load

provide a continuous stress distribution through the full length of the beam. This of course would be impossible. Guyon found by varying the size of the bearing plates that a corresponding change in transverse stress was obtained. A graph of transverse stress (fy) versus distance along OZ, for a symmetrical load arrangement, has been plotted for various bearing plate sizes, figure 4 .

Guyon continued his study of end blocks by applying loads at various positions across the bearing surface.

By replacing a single force by a number "n" of regularly spaced forces without modifying the bearing pressure on the surface to which the forces are applied, the maximum transverse tensile stress remains unchanged, but the length of the lead-in zone is divided by "n" as are the resultant tensile forces in a given region, hence the tensile reinforcement in that region.is also reduced.

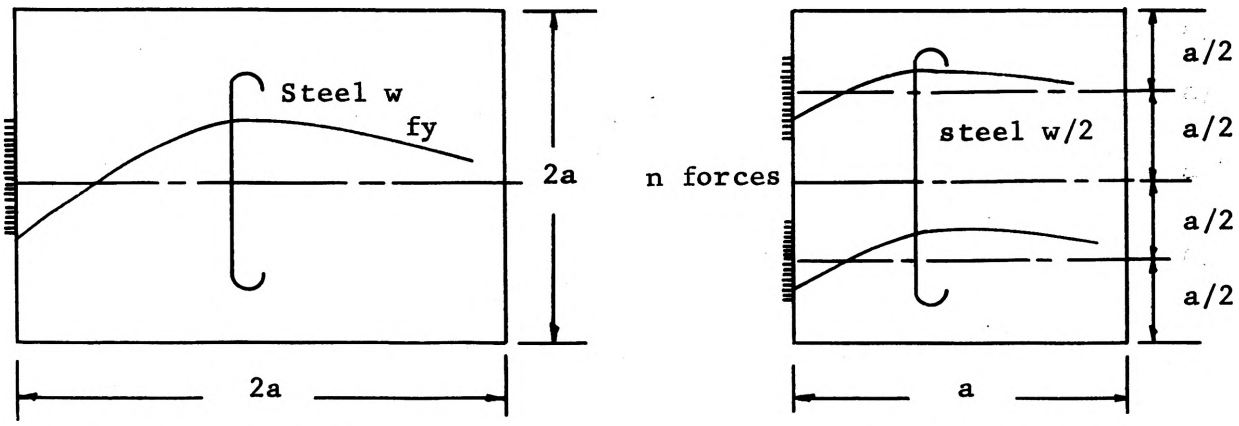

Singly Applied Force

Single Force Divided into Two Equal Forces

Tensile Reinforcement Required

Figure 5

The principal effect of localized forces is the production of stresses in planes at right angles to the line of action of forces and which tend to burst the element transversely to the direction of the applied force. To resist these stresses, reinforcement must be provided in planes parallel to the bearing surface. Such reinforcement is usually fitted in two mutually perpendicular directions, i.e., horizontal and vertical planes.

According to St. Venant's principle, the state of stress across transverse sections through a concrete member subjected to a number of localized forces on its ends is dependent only upon the magnitude, position and direction of the resultant of these forces and not upon the precise method of application of each individual force, provided that the sections are not close to the ends of the member. Stated another way, the effect of forces applied over a small area may be treated as a statically equivalent system which, at a distance approximately equal to the height of a beam, causes stress distribution which follows the simple law, = P/A.[5]

P. B. Morice and E. H. Cooley[6] attack this stress analysis problem by assuming that it is the same type problem as occurs in a design of a foundation block transmitting a number of concentrated loads to an elastic bearing medium. Figure 6. In general sections parallel to the lines of action of the prestressing forces are subjected to shear forces and bending moments, within the length of the lead-in zone.

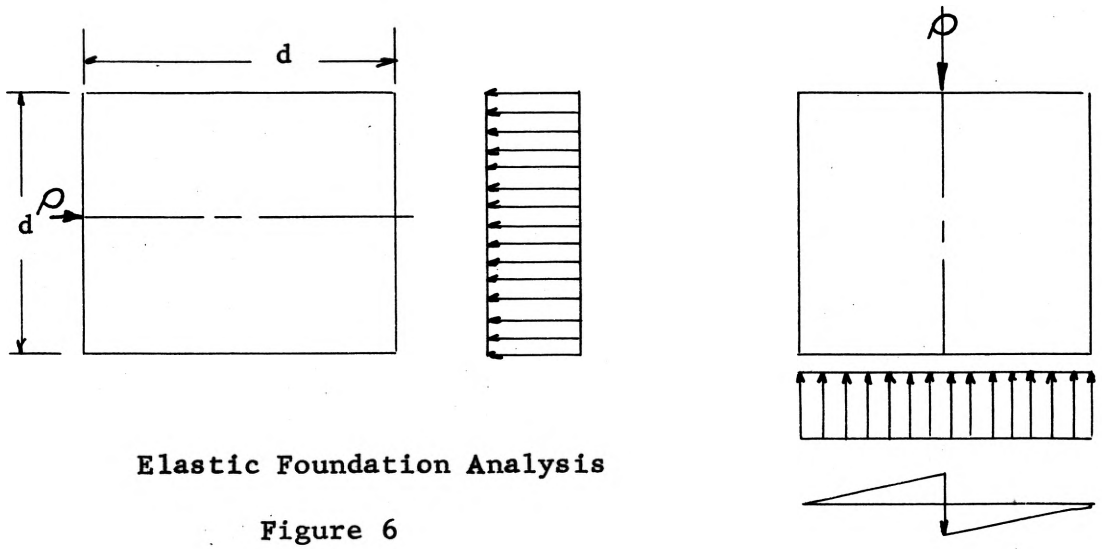

Elastic Foundation Analysis

Figure 6

Each set of end forces sets up a particular shear force and bending moment distribution in the end block. Those which tend to reduce the tensile stresses will provide a greater factor of safety against failure. Thus, without affecting the action of the rest of the beam the designer is free to choose his end forces as he pleases, provided the resultant of these forces has the desired magnitude, position and direction.(6)

The shear stresses produced on the vertical sections in the foundation block, combined with the transverse compressive and tensile stresses, induce greater principal stresses acting on planes inclined at an angle to the beam's axis.Therefore it is advantageous to reduce the shear in the end block to a minimum.

Magnel(7) approaches the stress problem from still a different angle that has the double advantage of being quick and erroring on the safe side by overestimating the maximum tensile stresses.

For the usual theory of bending, the assumption that the stress distribution is linear, is too inaccurate for stress analysis in end blocks assumed to be acting on a foundation. There is in reality, no definite underside to the foundation block; it continues past the assumed base as the remainder of the prestressed beam, and the transverse bending stresses will gradually die away.(6)

Magnel suggests a stress distribution of the form shown in Figure 7.

By assuming that the stress in the bottom of the block approaches zero tangentially (a gradual process), and by equating the areas of the compressive and tension zones, it is possible to obtain an equation for the shape of this non-linear stress distribution so that stress values can be obtained at various depths through the block. The bending stress at any point on a vertical plane through the foundation block is given by

$$C = K_1 \frac{M}{Ad}$$

where M is the bending moment acting on the plane under consideration, A is the area of the plane and d is its depth. K is a coefficient expressing the shape of the assumed stress distribution.(4)

The shear stresses at any point in the foundation block is distributed over a vertical section of the block in a manner that may be derived from the expression for the assumed bending stress distribution. The value of s at any point on a vertical plane through the foundation block is given by

$$S = K_2 \frac{S}{A}$$

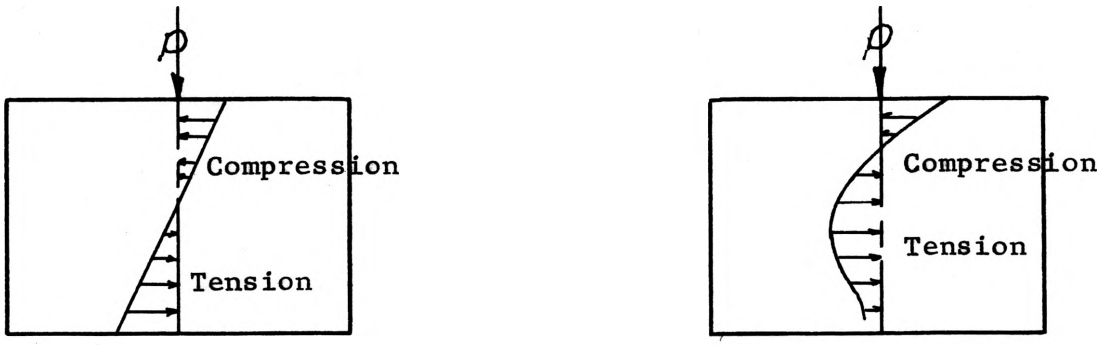

Normal Theory of Bending

According to Magnel

Bending Theory

Figure 7

where S is the shear force acting on the plane under consideration and A is the area of the plane. K is a coefficient expressing the shape of the shear-stress distribution corresponding to the depth from the top surface of the point required.(10)

Magnel has constructed a chart for these various coefficients of K with respect to the desired depth below the top of the foundation block.

The longitudinal compressive stress p is constant throughout the lead-in zone with the exception immediately below the prestressing force. See figure below:

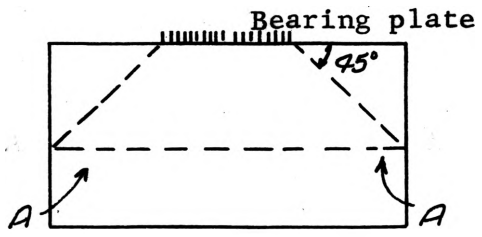

Stress Distribution

Figure 8

Magnel assumes the compressive stresses are dispersed along a 45 degree line from the edge of the base plate, as shown above. Therefore the area above the plane AA is reduced in comparison with the length width product. This results in a higher compressive value for p.

Through the use of Mohr's circle, Magnel calculates values for the principal tensile stresses from which steel reinforcement is designed.

Magnel compared theoretical data with tests run on end blocks in the laboratory. Calculations of tensile failure throughout the lead-in zone indicated that failure would occur at a somewhat greater depth than was found to exist by the laboratory results.

The material covered thus far has placed the emphasis on the transverse stresses and steel requirements. One other area which must not be overlooked is the steel required in the immediate vicinity of the prestressing force. The patented anchorage devices used will usually provide plans for wire cage reinforcement if imbedded in the concrete.

The steel reinforcement required in the spalling zone, (Figure 9) is usually determined by experience. The tensile stress that exists

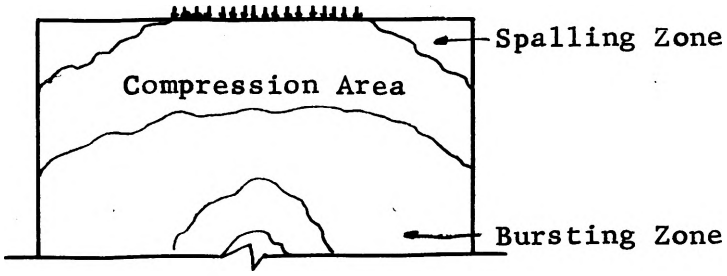

Figure 9

in this area must be resisted by steel. Even though steel may not be required, Magnel feels it is advisable to provide some mild steel so that in the event of subsequent damage to the end of the beam the anchorage zone would hold together and not disintegrate completely.

PHOTOELASTICITY

In 1816, Sir David Brewster, a British physicist, discovered that when a piece of glass was stressed and viewed by polarized light passing through it, a fringe pattern was set up, Figure 14. He suggested that the fringe pattern might serve as a basis for measurement of stress in engineering structures. Very little was done experimentally from the time of Brewster until the beginning of the twentieth century to utilize his knowledge for design purposes.(8)

The science of photoelasticity moved from this undeveloped stage to the practical stage, mainly by the persistent and life-long labors of Professor E. G. Coker and the late L. N. G. Filon, both of the University of London. Their Treastise on Photoelasticity was published in 1930 by the Cambridge Press. Since then there have been improvements made on technique and materials, and the science has been extended into the three dimensional field. Today Photoelasticity is one of the cheapest, most accurate and versatile of the methods available to the stress analysts.

The ultimate objective of any stress analysis study is the determination of the state of stress in the structure being investigated with sufficient accuracy and at enough points to provide information for an adequate design.

The photoelastic method involves making a transparent plastic model and determining stresses in this model under a simulated load. This method has an advantage over the strain gage technique in that stresses may be calculated at every point in the model rather than at the specific point where strain gages are located.(9)

Certain transparent materials such as crystals of calcite and mica or certain strained plastics demonstrate the phenomenon of double-refraction. Double-refraction divides a ray of light into two beams, which travel at different speeds through the material. This means that one beam will be retarded in relation to the other while traveling through the plastic. The two beams of light transmitted through the double-refractive materials are polarized at right angles to each other. The direction of polarization corresponds to the direction of principal strains in the double-refractive material.(10)

Stress is induced into the model (double-refractive material) by the application of a load. This stress pattern set up is in the form of dark or bright bands, (Figure 14). These black bands are known as fringes. In terms of stress a fringe becomes the locus of points of constant difference between the principal stresses P and Q. This is a result of double-refraction.(10)

The mathematical equations, to be used in the calibration of the double-refractive material, are listed as follows:

$$\tau_{max} = \frac{P-Q}{2} \qquad (1)$$

$$Ft = f^{?} \qquad (2)$$

$$F_{\sigma} = \tau_{max} \qquad (3)$$

$$\sigma = \frac{My}{I} \qquad (4)$$

Equation (1) gives the relationship of the principal stresses to the maximum shear stress. τ max is equal to the maximum shearing stress, P is equal to one principal stress and Q is equal to the other principal stress.

Equations (2) and (3) are used to relate the difference in principal stress to the various properties of the model used. The model fringe value "F", depends on the kind of material used, its thickness, t, and the wave length of the light employed. The material fringe value is represented by "f".

Equation (4) is the flexure formula that will be used later to obtain the model and material fringe values.

In order to check Guyon and Magnel's analytical calculations, of transverse tensile stress in the vicinity of the applied load by photoelasticity, a two dimensional stress investigation will be made.

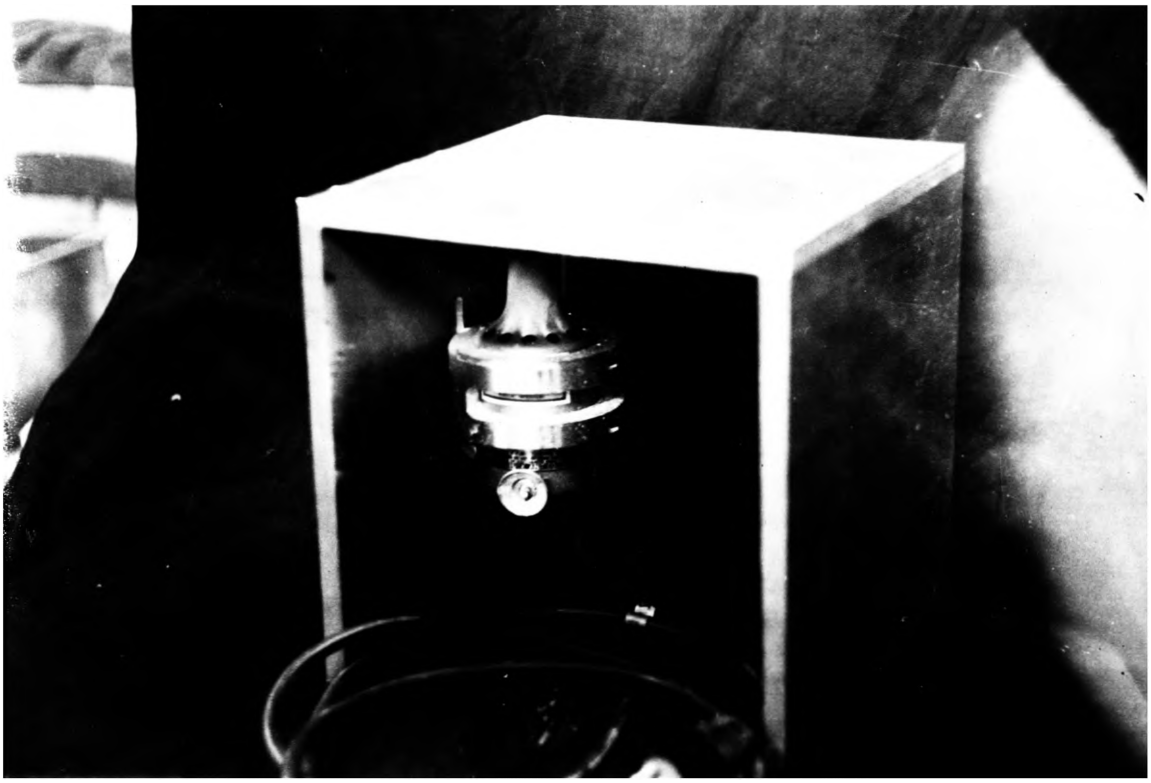

High Speed Milling Machine

Figure 10

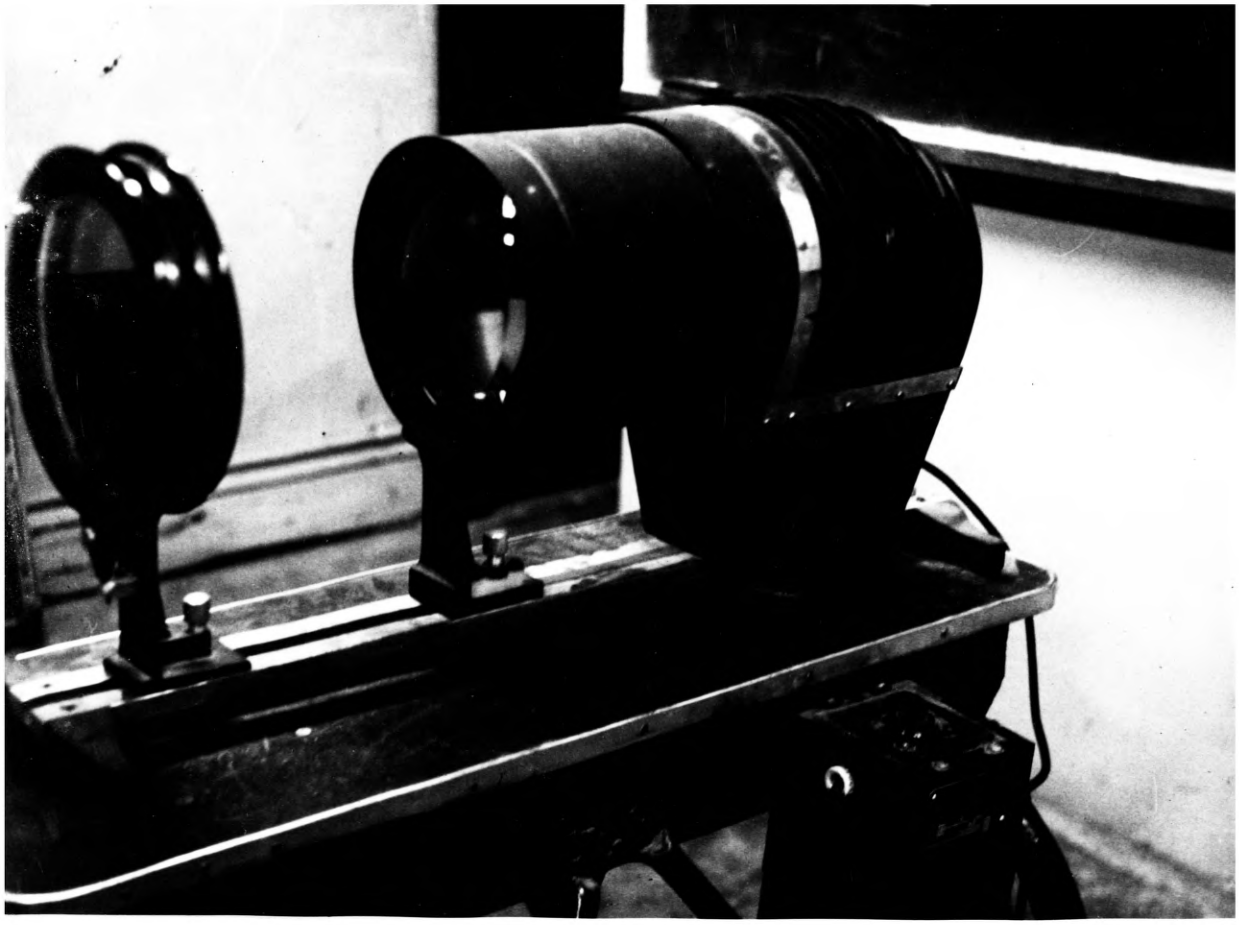

Light Source

Figure 11

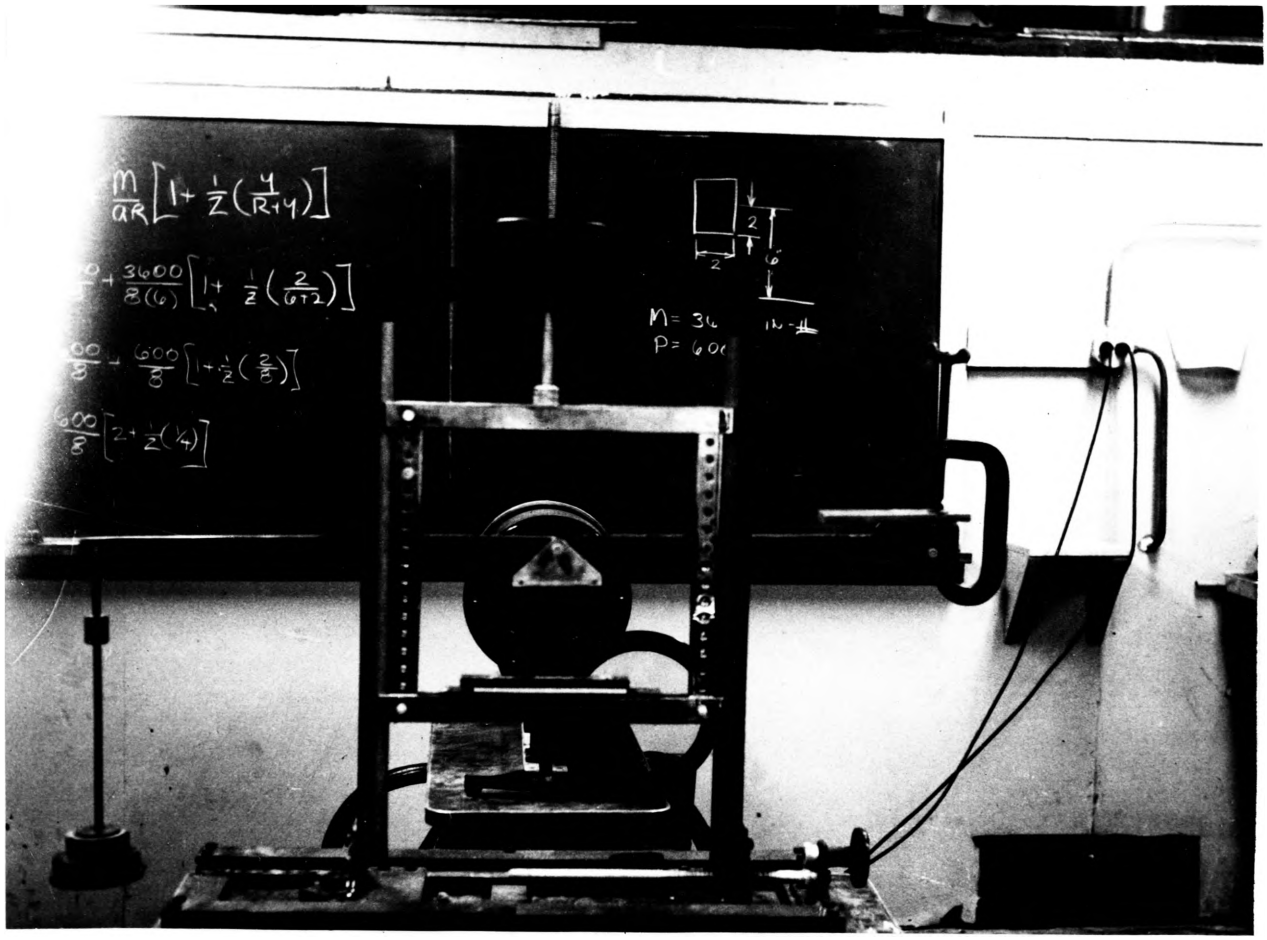

Guillotine Type Loading Frame

Figure 12

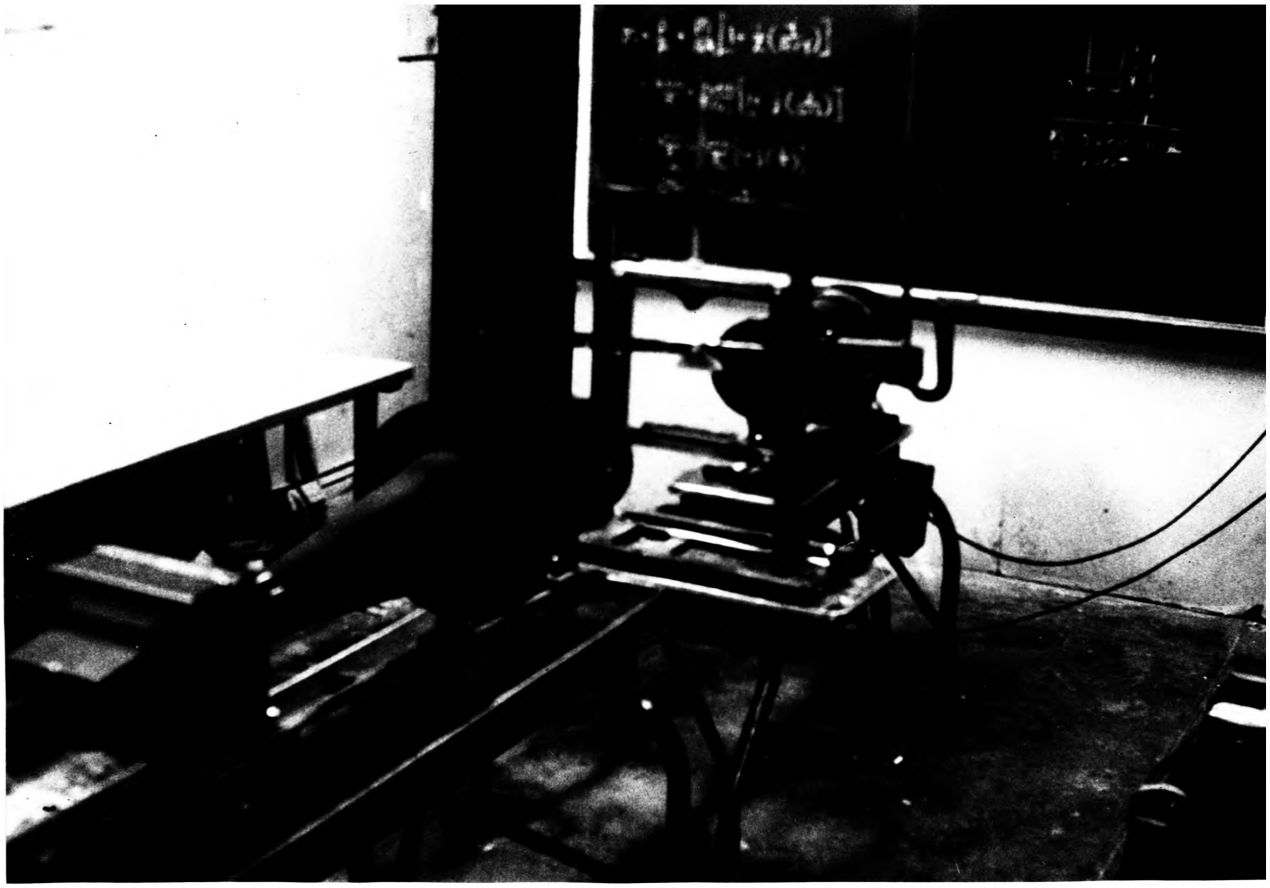

Polaroids and Quarter Wave Plates

Figure 13

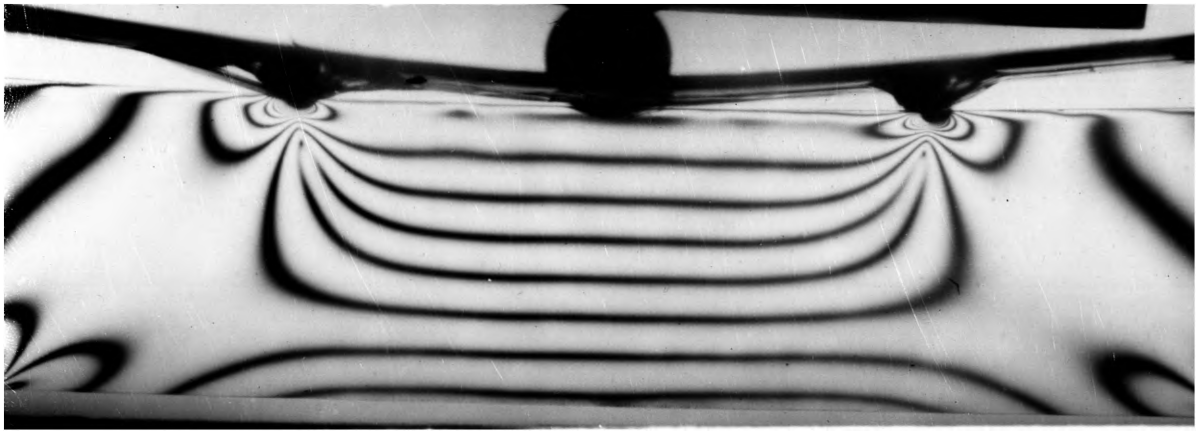

Stress Pattern Beam in Pure Bending

Figure 14

EXPERIMENTAL MODEL ANALYSIS

The problems that produced the greatest difficulties were in the making and loading of the model. It was necessary that the concentrated load be a vertical load and that it be symmetrically placed, with respect to the cross sectional area, in order to produce fringes symmetrical about the axis of loading. Care was exercised when grinding in order to prevent residual stresses. Scratches on the face of the model were avoided as they could lead to stress concentration which would result in incorrect data.

The double-refractive material used in this model analysis was taken from a sheet of Columbia Resin, referred to as CR 39, of 1/4 inch nominal thickness. Actual thickness was 0.247 inches. CR 39 is a beautifully clear material having about the same optical sensitivity as Bakelite but about half the modulus of elasticity. It cannot be welded satisfactory and is hard to machine owing to the tendency to chip along the edges because of brittleness. The grinder used was a high speed milling machine, mounted in a specially built aluminum stand resting on top of a work bench, figure 10. The template used in making the model was cut from a piece of aluminum 0.124 inches thick.

The polariscope was equipped with two polaroids, two-quarter wave plates, figure 13, a mercury-vapor monochromatic light source, figure 11, a white light source, a guillotine type loading frame, figure 12, a Wratten-77 filter, and a camera. The camera was of the bellows type and was equipped with a standard 5 x 7 film holder, figure 13.

Calibration Test:

The material fringe value (f) and the model fringe value (F) were determined by means of a calibration test in pure bending. An illustration of the loading frame and the beam is pure bending is shown in figure 15.

As the load on the calibration beam was gradually increased, fringes began to appear. The loads that produced increments of half and whole fringes were recorded. The half fringe was obtained from a mixed-set-up which produce a white background, figure 16. The whole fringe was obtained with a crossed-set-up which produced a black background, figure 17.

A look at the moment and shear diagram of the model, figure 15, indicates that within the region A-B, the bending moment is constant, there is no vertical or horizontal shear stress, and the normal stress to the element shown is zero. Therefore from this boundary condition, $\sigma_y = 0$ and σ_x will be equal to the principal stress, P.

From equations 1-4

$$\frac{P-q}{2} = \tau_{max}; \qquad \sigma_y = 0, \ \sigma_x = P \qquad \therefore \tau_{max} = P/2$$

$$\sigma_x = P = \frac{M_y}{I} \qquad \tau_{max} = \frac{M_y}{2I} = nF$$

$$F = \frac{M_y}{2I} \cdot \frac{1}{n} = \frac{\sigma_x}{2} \cdot \frac{1}{n}$$

The model fringe value (F) is represented by the slope of a curve of τ_{max} versus fringe number, figure 18.

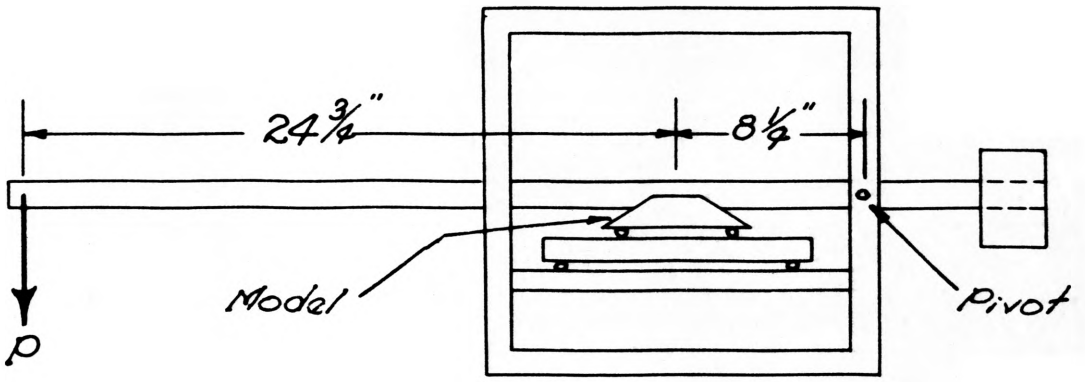

Guillotine Type Floating Frame

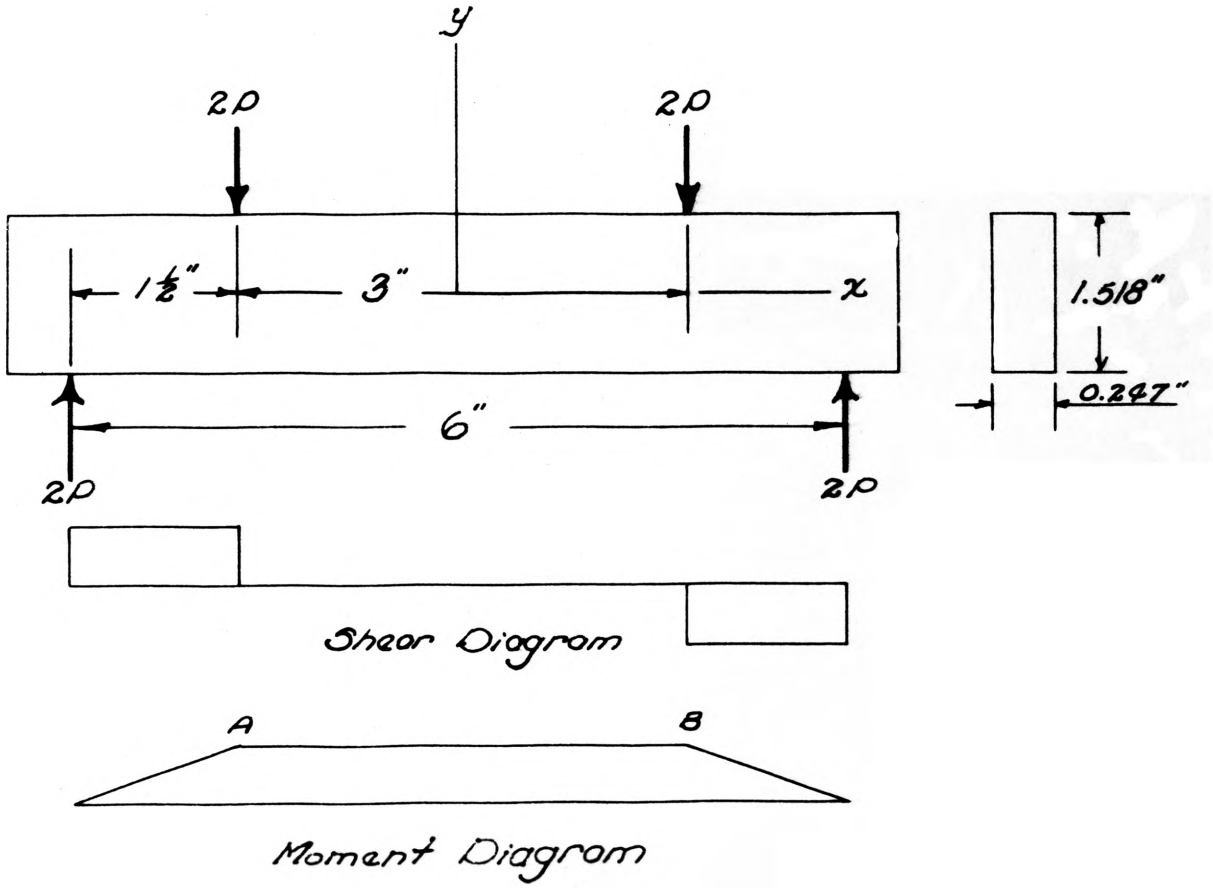

Beam in pure Bending

Figure (15)

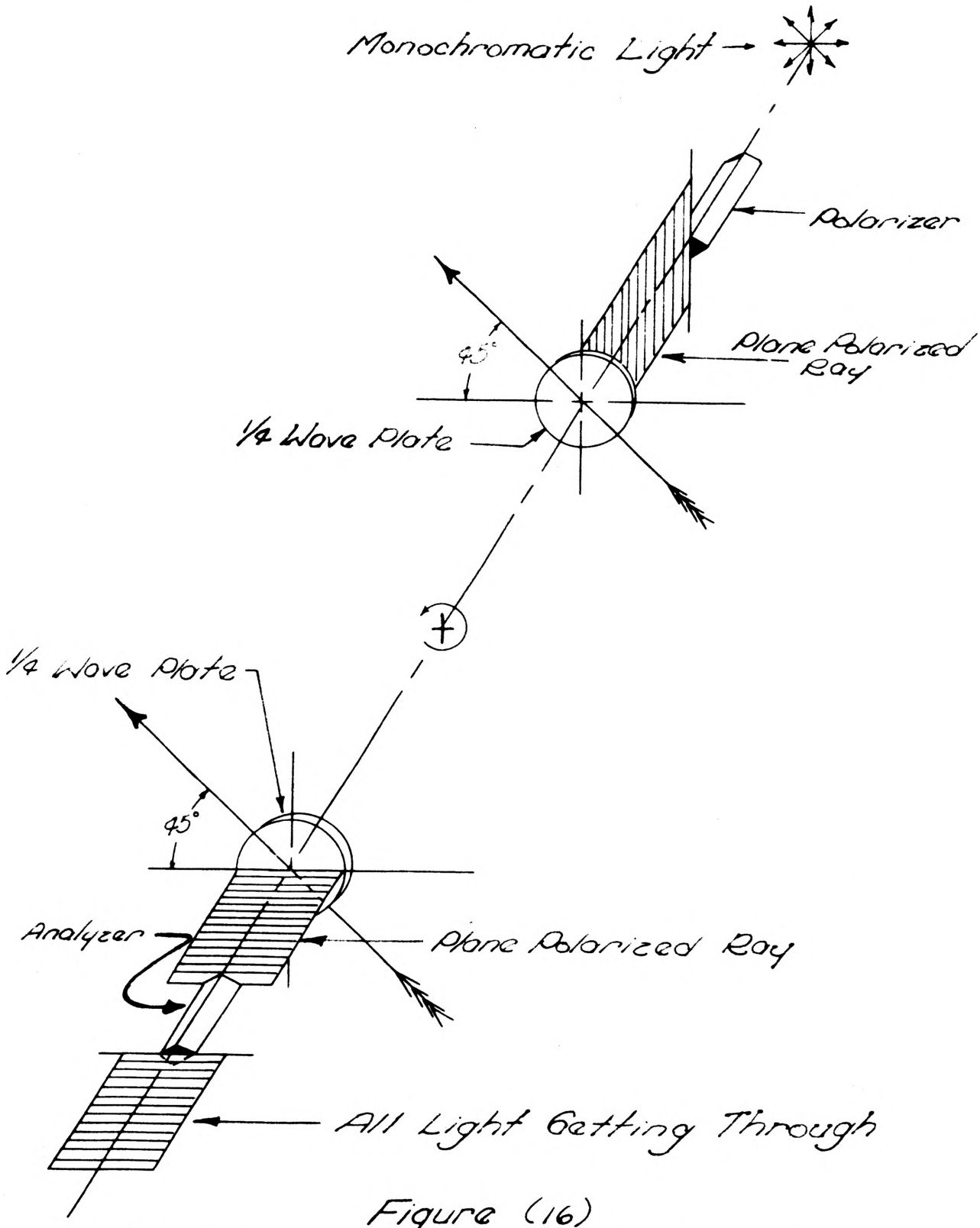

Figure (16)

M.M. Frocht, "Photoelasticity" Page 126

Mixed Set-up

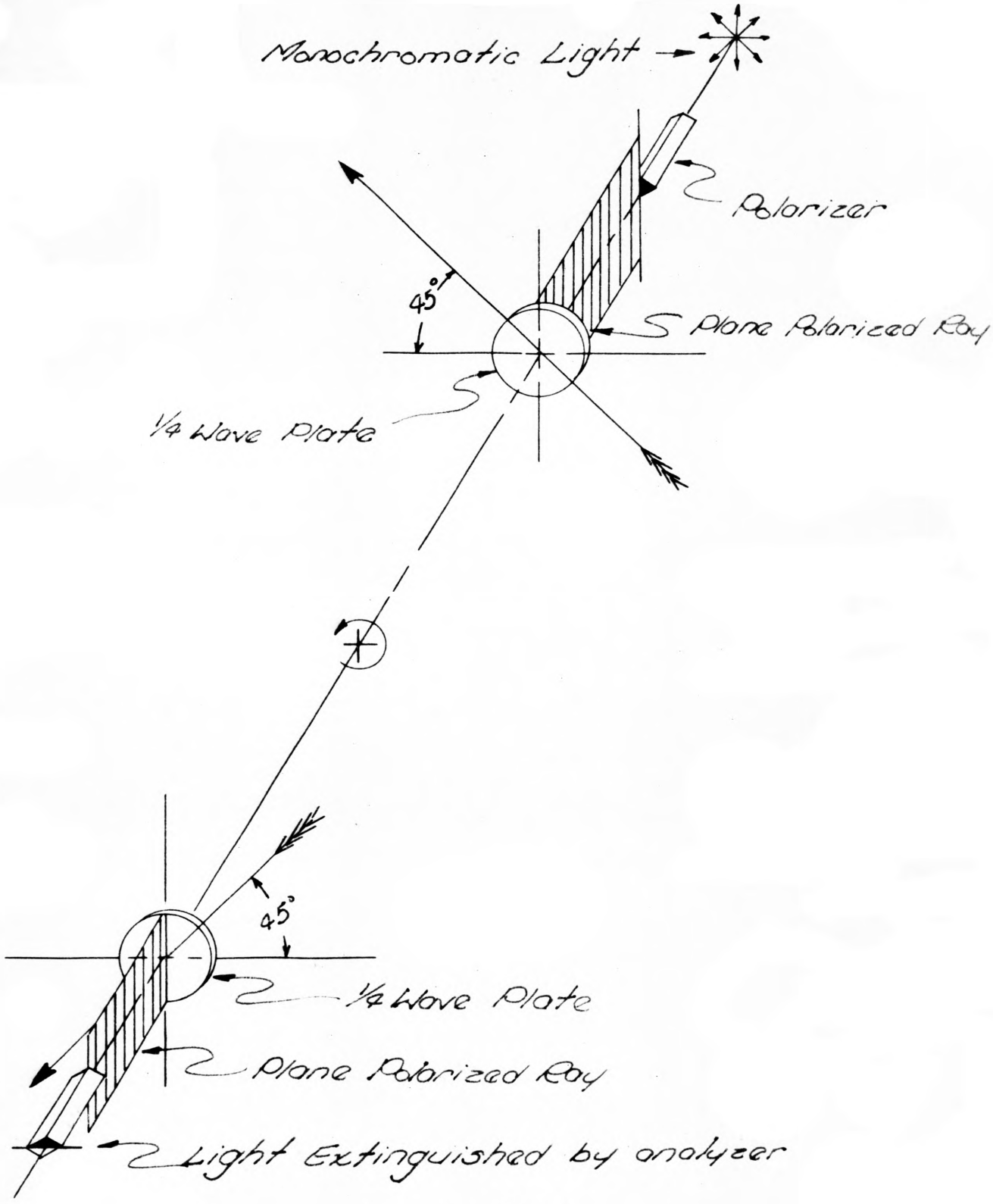

Figure (17)

M. M. Frocht Photoelasticity Page 126

Crossed Circular Polariscope

Calibration Data

Load (2P)	Fringe Number	Moment	$\frac{My}{I}$	$\frac{\sigma_x}{2} = \tau_{max}$
11.0	1/2	16.5	175	87.5
22.2	1	33.3	353	177.0
35.0	1 1/2	52.5	556	278.0
44.0	2	66.0	700	350.0
56.0	2 1/2	84.0	890	445.0
66.0	3	99.0	1050	525.0
76.8	3 1/2	115.0	1220	610.0

From Figure (18):

Model Fringe Value (F)

$$F = \frac{\Delta \tau_{max}}{\Delta n} = \frac{443}{2.5} = 177.5$$

Material Fringe Value (f)

$$f = t F = (0.247)(177.5) = 43.8$$

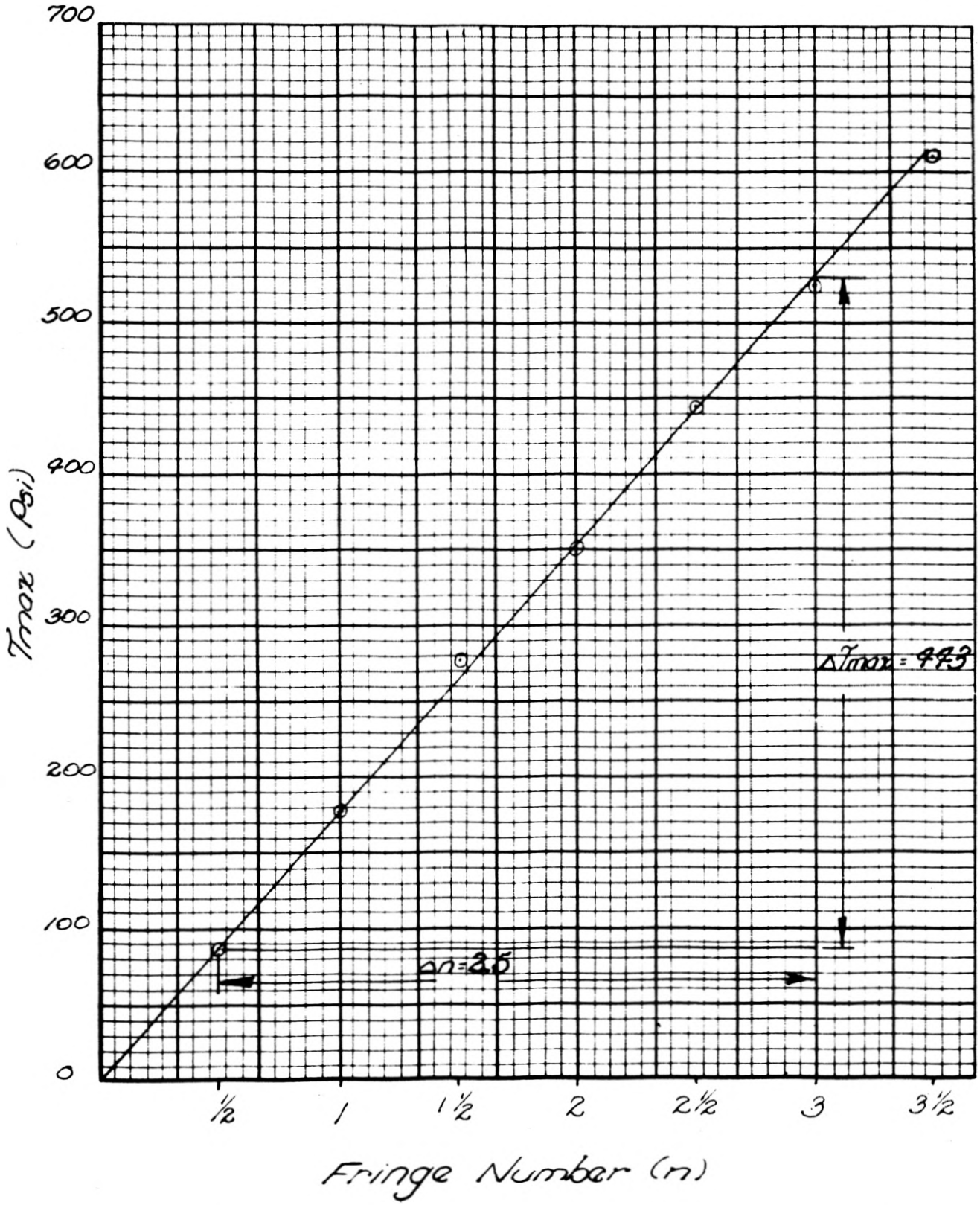

Graph of: Tmax (Psi) versus Fringe Number (n)

Figure (18)

Determination of Tensile Stresses

The photoelastic model of the lead-in zone was symmetrically loaded with a concentrated load. The load produced fringes that crossed the symmetrical axis at various depths, figures 19 and 20. The picture of the isoclinics - the locus of points along which the principal stresses have parallel directions - figure 21, indicates that the zero degree isoclinic coincides with the symmetrical axis. Therefore the stresses along this axis are principal stresses. Within the immediate vicinity of the load, these fringes could not be distinguished.

At the point of application, under high stress concentration, there is always a certain plastic yielding of the material and as a result of this yielding the load will become distributed over a finite area. Imagine that the portion of material which suffered a plastic flow is cut out from the model by a circular cylinder surface of small radius. Then the equations of elasticity can be applied to the remaining portion of the model.(11)

At points along the symmetrical axis, where fringes cross, the difference in principal stresses (P-Q) is known. The transverse stresses cannot be determined until a separation in (P-Q) has been made.

Several methods are available for the separation of P and Q stresses. The methods of separation are not dependent on maintaining purely elastic conditions, although the experimental data from which this analysis was made were obtained from a photoelastic model which should be kept within the elastic range for the data to be usable. The method chosen is known as the Shear Difference Method, developed by M. M. Frocht.(10)

The Shear Difference Method is a numerical method of integration. The value of this integral can be represented by the area under a curve for which the ordinates are the "rate of change of shear in a direction normal to direction of integration" and the abscissas are directions along the path of integration.(12)

For two dimensional stress states the equations of equilibrium are as follows:

$$\frac{\delta \sigma_x}{\delta x} + \frac{\delta \tau_{xy}}{\delta y} + X = 0 \qquad (1)$$

$$\frac{\delta \sigma_y}{\delta y} + \frac{\delta \tau_{xy}}{\delta x} + Y = 0 \qquad (2)$$

where σ_x and σ_y are the normal stresses on the x and y planes, τ_{xy} is the shearing stress intensity on the x and y planes, and X and Y are body forces per unit volume in the x and y direction.(12) The body forces can be neglected since their influence is usually small in comparison with the effect of the applied load.

By multiplying both sides of equation (1) by dx and integrating with respect to x, the equation reduces to:

$$\sigma_x = (\sigma_x)_o - \int \frac{\delta \tau_{xy}}{\delta y} dx \qquad (3)$$

where $(\sigma_x)_o$ represents the value of σ_x at a given location for which the stress values are known or may be obtained. In this problem the stress in the x direction is known at the boundary.

In the case of a small finite particle, equation (3) which contains integrals, can be closely approximated by the following expressions containing summations of finite increments:

$$\sigma_x = (\sigma_x)_o - \sum \frac{\Delta \tau_{xy}}{\Delta y} \Delta x \qquad (4)$$

Equation (4) can be reduced further by making increments such that Δx equals Δy :

$$\sigma_x = (\sigma_x)_o - \sum \Delta \tau_{xy} \qquad (5)$$

The shear stress on any x-y plane in terms of fringe number and model fringe value, is represented by the following equation:

$$\tau_{xy} = nF \sin 2\theta$$

in terms of principal stresses

$$\tau_{xy} = \frac{p-q}{2} \sin 2\theta$$

In order to determine the maximum tensile transverse stress along the axis of the applied load, several sections were chosen to apply the Shear Difference Method, figures 20 and 21. Once these principal stresses were separated, a graph of transverse stress versus distance along the symmetrical axis, was plotted, figure 22.

Fringe Pattern (Concentrated Load)

Figure 19

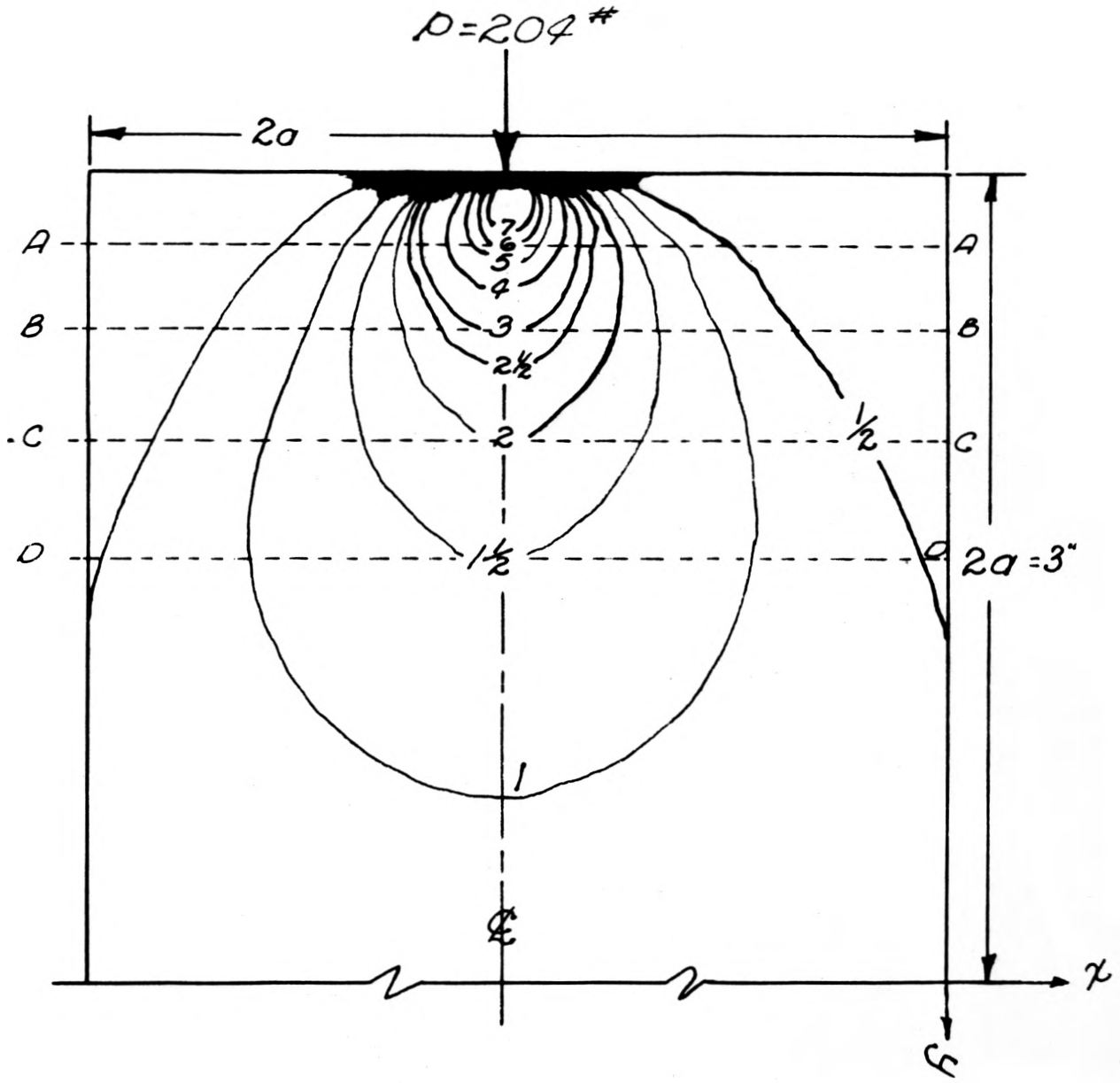

Fringe Pattern
Simulated Lead-in Zone (CR-39)

Figure (20)

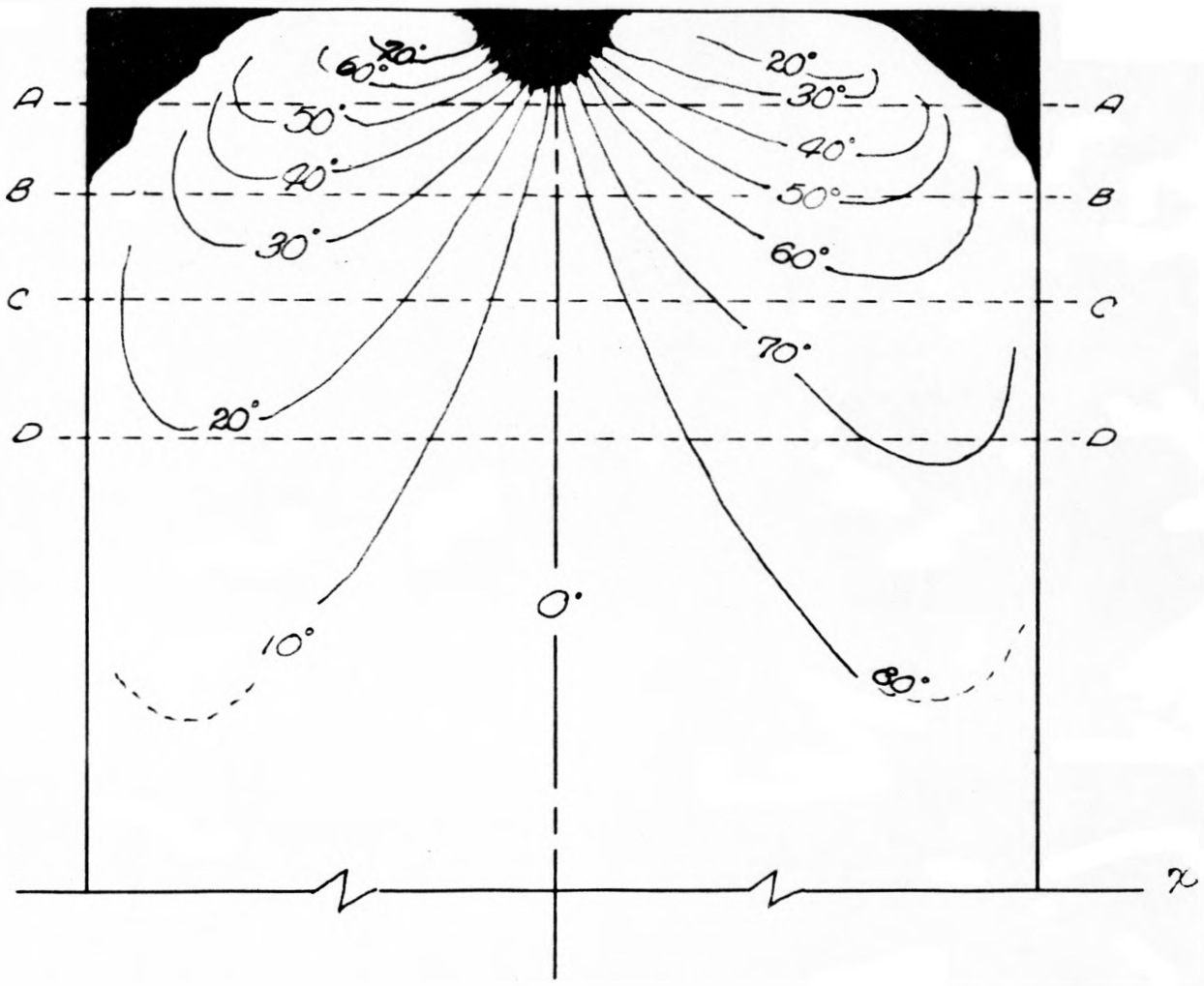

Isoclinics

Simulated Lead-in Zone (CE 39)

Figure (21)

Experimental Data

Section A-A (Figures 19 and 20)

Depth	Location	Fringe Number(n)	Model Fringe(F)	Sin 2 θ	Txy (psi)	Txy (psi)
0.1D	Point 1	0.09	177.5	θ = 80° 0.34	5.5	47.8
	Point 2	0.30	177.5	θ = 45° 1.00	53.3	
0.2D	Point 3	0.20	177.5	θ = 15° 0.50	17.8	63.8
	Point 4	0.50	177.5	θ = 33° 0.92	81.6	
0.3D	Point 5	0.48	177.5	θ = 20° 0.642	54.6	153.4
	Point 6	1.20	177.5	θ = 43° 0.927	208	
0.4D	Point 7	2.10	177.5	θ = 30° 0.864	322	37
	Point 8	2.30	177.5	θ = 59° 0.88	359	
0.5D	Point 9	Unknown	177.5	0	0	0
	Point 10	3.8	177.5	0	0	

Experimental Data

Section A-A (Figures 19 and 20)

Depth	Fringe Number(n)	2F	(P-Q) (psi)	$\frac{(P-Q)}{2}$ (psi)	θ	Sin 2 θ	Txy (psi)
0	0.09	356	32	16	90^{o}	0	0
0.1D	0.20	356	71.5	35.3	62.5^{o}	0.82	28.9
0.2D	0.40	356	142	71	27^{o}	0.81	57.6
0.3D	0.84	356	299	149	31.5^{o}	0.89	133
0.4D	2.15	356	766	383	44.5^{o}	0.999	300
0.5D	6	356	2140	1070	0	0	0

Experimental Data

Section A-A (Figures 19 and 20)

Depth	Mean $\frac{(\Delta x)}{Txy(\Delta y)}$	σ_x (psi)	(P-Q) (psi)	Txy psi	$(P-Q)^2$	$4\ Txy^2$	$\sqrt{(P-Q)^2 - 4\ Txy^2}$	σ_y psi
0	---	0	32	0	1024	0	32	-32
0.1D	47.8	-47.8	71.5	28.9	5110	3340	42	-89.8
0.2D	63.8	-111.6	142	57.6	20,200	13,300	83	-19.46
0.3D	153.4	-265.0	299	133	89,400	70,800	136	-401
0.4D	37	-302.0	766	300	586,000	360,000	475	-177
0.5D	0	-302	2140	0	4,590,000	0	2140	-244.3

Experimental Data

Section B-B (Figures 19 and 20)

Depth	Location	Fringe Number(n)	Model Fringe(F)	Sin 2 θ	Txy (psi)	Txy (psi)
0.1D	Point 1	0.30	177.5	θ = 45° 1	63.3	21
	Point 2	0.45	177.5	θ = 56° 0.926	74	
0.2D	Point 3	0.5	177.5	θ = 27° 0.81	72	61
	Point 4	0.8	177.5	θ = 55° 0.94	133	
0.3D	Point 5	1.1	177.5	θ = 43° 0.996	195	18
	Point 6	1.4	177.5	θ = 60° 0.866	213	
0.4D	Point 7	2.3	177.5	θ = 60° 0.866	350	122
	Point 8	2.0	177.5	θ = 70° 0.643	228	
0.5D	Point 9	4.0	177.5	θ = 1° .0349	24.6	-9.5
	Point 10	2.45	177.5	θ = 1° .0349	15.1	

Experimental Data

Section B-B (Figures 19 and 20)

Depth	Fringe Number(n)	2F	(P-Q) (psi)	$\frac{(P-Q)}{2}$ (psi)	θ	Sin 2 θ	Txy (psi)
0	0.23	356	82	41	90^{o}	0	0
0.1D	0.38	356	135	67.5	52^{o}	0.97	65.5
0.2D	1.00	356	356	178	48^{o}	0.99	176
0.3D	1.25	356	445	222	51^{o}	0.97	215
0.4D	2.2	356	782	391	65^{o}	0.766	300
0.5D	3.0	356	1070	535	0	0	0

Experimental Data

Section B-B (Figures 19 and 20)

Depth	Mean $\frac{(\Delta x)}{Txy(\Delta y)}$	σ_x (psi)	(P-Q) (psi)	Txy psi	$(P-Q)^2$	$4\ Txy^2$	$\sqrt{(P-Q)^2 - 4Txy^2}$	σ_y psi
0	---	0	82	0	6730	0	82	-82
0.1D	+21	-21	135	65.5	18,210	17,100	33	-54
0.2D	+61	-82	356	176	127,000	124,000	54.8	-115.8
0.3D	+18	-100	445	215	198,000	185,000	114	-214
0.4D	-122	+22	782	500	612,000	360,000	502	-480
0.5D	-9.5	_31.5	1070	0	1,142,000	0	1070	-1038.5

Experimental Data

Section C-C (Figures 19 and 20)

Depth	Location	Fringe Number(n)	Model Fringe(F)	Sin 2 θ	Txy (psi)	Txy (psi)
0.1D	Point 1	0.48	177.5	$\theta = 60^{\circ}$ 0.866	74	17
	Point 2	0.65	177.5	$\theta = 64^{\circ}$ 0.788	91	
0.2D	Point 3	0.80	177.5	$\theta = 59^{\circ}$ 0.88	125	-7
	Point 4	0.90	177.5	$\theta = 66^{\circ}$ 0.74	118	
0.3D	Point 5	1.30	177.5	$\theta = 63^{\circ}$ 0.81	187	-49
	Point 6	1.25	177.5	$\theta = 71^{\circ}$ 0.62	138	
0.4D	Point 7	1.95	177.5	$\theta = 72^{\circ}$ 0.586	203	-80
	Point 8	1.70	177.5	$\theta = 78^{\circ}$ 0.406	128	
0.5D	Point 9	2.4	177.5	$\theta = 1^{\circ}$ .0349	14.8	-6.5
	Point 10	2.0	177.5	$\theta = 1^{\circ}$ .0349	12.3	

Experimental Data

Section C-C (Figures 19 and 20)

Depth	Fringe Number(n)	2F	(P-Q) (psi)	$\frac{(P-Q)}{2}$ (psi)	θ	Sin 2 θ	Txy (psi)
0	0.38	356	135	68	90^{o}	0	0
0.1D	0.60	356	214	107	62^{o}	0.83	89
0.2D	0.80	356	285	143	65^{o}	0.766	111
0.3D	1.30	356	463	231	71^{o}	0.615	142
0.4D	1.75	356	623	312	79^{o}	0.375	117
0.5D	2.0	356	713	357	0	0	0

Experimental Data

Section C-C (Figures 19 and 20)

Depth	Mean $\frac{(\Delta x)}{Txy(\Delta y)}$	σ_x (psi)	(P-Q) (psi)	Txy psi	$(P-Q)^2$	$4\ Txy^2$	$\sqrt{(P-Q)^2 - 4Txy^2}$	σ_y psi
0	---	0	135	0	18,200	0	135	0
0.1D	+17	-17	214	89	45,800	31,700	118.8	-135.8
0.2D	-7	-10	285	111	81,000	49,300	178	-188
0.3D	-49	+39	463	142	214,000	81,000	365	-324
0.4D	-80	+119	625	117	391,000	54,700	580	-461
0.5D	-6.5	+125.5	713	0	509,000	0	713	-587.5

Experimental Data

Section D-D (Figures 19 and 20)

Depth	Location	Fringe Number(n)	Model Fringe(F)	Sin 2 θ	Txy (psi)	Txy (psi)
0.1D	Point 1	0.65	177.5	θ = 66° 0.74	85	-9
	Point 2	0.70	177.5	θ = 71° 0.61	76	
0.2D	Point 3	0.95	177.5	θ = 68° 0.696	117	-25
	Point 4	0.88	177.5	θ = 72° 0.59	92	
0.3D	Point 5	1.25	177.5	θ = 74° 0.53	118	-32
	Point 6	1.10	177.5	θ = 77° 0.44	86	
0.4D	Point 7	1.50	177.5	θ = 81° 0.31	82	-27
	Point 8	1.30	177.5	θ = 83° 0.24	55	
0.5D	Point 9	1.70	177.5	θ=1° .0349	10.4	-1.5
	Point 10	1.44	177.5	θ = 1° .0349	8.9	

Experimental Data

Section D-D (Figures 19 and 20)

Depth	Fringe Number(n)	2F	(P-Q) (psi)	$\frac{(P-Q)}{2}$ (psi)	θ	Sin 2 θ	Txy (psi)
0	0.40	356	142	71	90^{o}	0	0
0.1D	0.68	356	242	121	68^{o}	0.695	84
0.2D	0.90	356	321	160	72^{o}	0.586	94
0.3D	1.20	356	427	213	76^{o}	0.470	100
0.4D	1.45	356	517	258	81^{o}	0.310	80
0.5D	1.50	356	535	268	0	0	0

Experimental Data

Section D-D (Figures 19 and 20)

Depth	Mean $\frac{(\Delta x)}{Txy(\Delta y)}$	σ_x (psi)	(P-Q) (psi)	Txy psi	$(P-Q)^2$	$4Txy^2$	$\sqrt{(P-Q)^2 - 4\ Txy^2}$	σ_y psi
0	---	0	171	0	29,200	0	142	-142
0.1D	-9	+9	242	84	58,500	28,300	174	-165
0.2D	-25	+34	321	94	103,000	35,500	260	-226
0.3D	-32	+66	427	100	182,000	40,000	403	-337
0.4D	-27	+93	517	80	267,000	25,600	491	-398
0.5D	-1.9	+94.9	535	0	286,000	0	535	-441.8

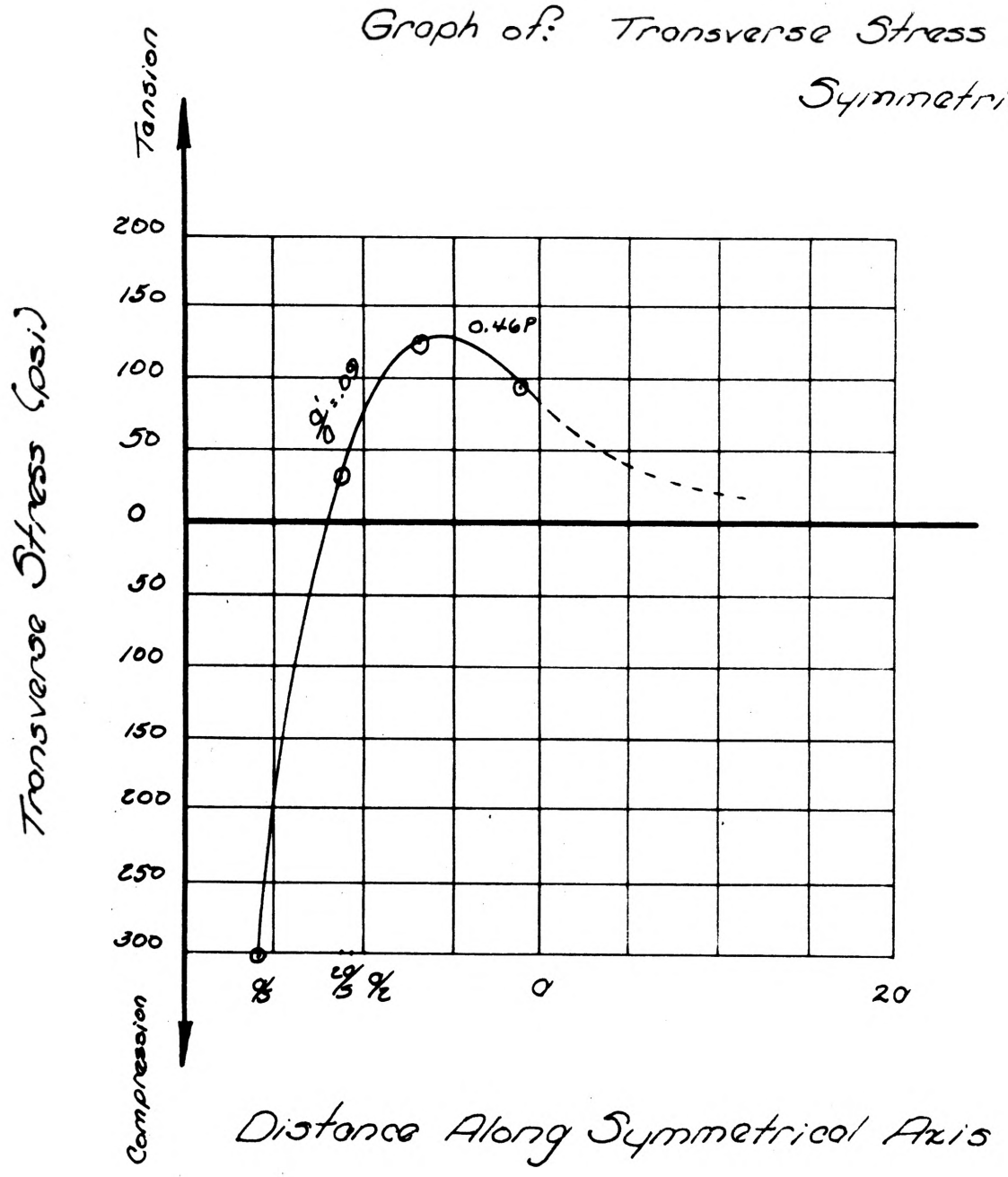
Graph of: Transverse Stress vs Distance Along Symmetrical Axis
Tension
200
150
100
50
0
50
100
150
200
250
300
Compression
Transverse Stress (psi)
0.46P
x = 0
x
0
20
Distance Along Symmetrical Axis

Figure (22)

Transition from Model to Prototype

In a two-dimensional stress system the stress distribution is generally independent of the physical constants so long as the materials are homogeneous and isotropic, the body either free from or subjected to constant body forces, and the stresses are within the elastic limit.(10)

The stress in the model is proportional to the load and inversely proportional to the depth and width:

$$\sigma_m \propto \frac{P_m}{d_m t_m}$$

Similarly the stress in the prototype is:

$$\sigma_p \propto \frac{P_p}{d_p t_p}$$

The transition from model to prototype can be made by dividing the stress in the prototype by the stress in the model:

$$\frac{\sigma_p}{\sigma_m} = \frac{\frac{P_p}{d_p t_p}}{\frac{P_m}{d_m t_m}} \; ; \qquad \sigma_p = \sigma_m \frac{d_m t_m}{d_p t_p} \cdot \frac{P_p}{P_m} \qquad (A)$$

In order to compare stress values obtained by the transition formula (A), with stress values found by Guyon, a factor "K" must be multiplied times the right hand side of equation (A):

$$\sigma_p = K \cdot \sigma_m \cdot \frac{d_m t_m}{d_p t_p} \cdot \frac{P_p}{P_m}$$

where "K" is the ratio of the average stress obtained by Guyon, with the use of strain gages placed throughout the end block of prestressed concrete beam, to the average stress obtained by the photoelastic analysis on the CR 39 end block.

$$K = \frac{0.42}{0.46} = \frac{(1)}{(1.1)}$$

REINFORCING REQUIRED IN END ZONE

The following example problem illustrates the use of stress values, found by the photoelastic method, in determining the transverse tensile reinforcement required in the end zone.

Example: Design the reinforcing steel required in the end zone of a post tensioned beam under the following conditions:

(1) Initial load on tendons - 200 kips

(2) Maximum allowable concrete stress in tension 120 psi.

(3) Beam height 30 inches, width 10 inches.

From transit formula (A):

$$\sigma_p = \sigma_m \frac{t_m d_m}{t_p d_p} \cdot \frac{A_p}{A_m} \cdot K$$

$$= \frac{(125)(3)(0.247)}{(10)(30)} \frac{209000}{204} \frac{1}{1.1}$$

$$= 275 \text{ psi}$$

For the portion of the beam whose stress exceeds the 120 psi allowable, reinforcing steel is needed.

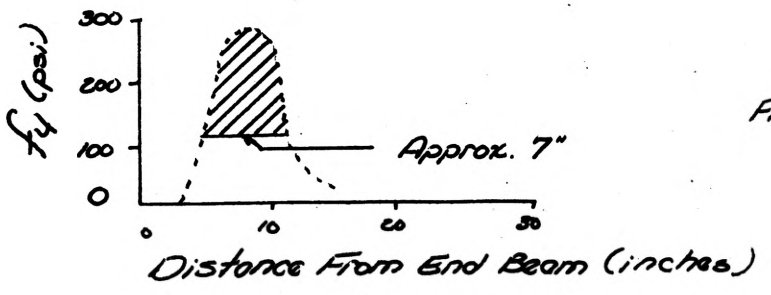

Figure (23)

Assuming an average stress of 145 psi.

The total tensile force to be resisted by steel:

$$(7)(10)(145) = 10,150^{\#}$$

For an allowable stress of 20,000 psi in the steel, the area of steel required is:

$$A_s = \frac{10,150}{20,000} = 0.506^{\#/"}$$

Four 1/2 inch stirrups spaced at 2 inch centers would be sufficient.

CONCLUSIONS AND RECOMMENDATIONS

Based on the author's library research of all available sources of information and the model analysis conducted with the use of photoelasticity, the following conclusions are presented.

(1) Very little has been done on the model analysis of prestressed concrete end blocks with the use of photoelasticity. The material available has been largely obtained from models made of concrete, the same material as the prototype.

(2) The photoelastic method provides a very accurate and economical means of obtaining stress values at an unlimited number of points.

(3) The fringe pattern within the immediate vicinity of the concentrated load was blurred making it impossible to determine the separate fringe order. In order to obtain a sufficient number of fringes, from which stress values were calculated, a large load was necessary which resulted in a plastic condition immediately below the load.

(4) The transverse stress along the axis of the applied load, was found to be compressive for a distance of approximately 2a/5 below the load and then changing to tension for the remainder of the length of the end block. The original idea was to apply a point load, but when the load was applied it had a small width which resulted in a bearing plate type loading instead of a point load.

(5) The Shear Difference Method of separating the principal stresses is largely dependent upon the accuracy of the location of the isoclinics and fringe orders. Small errors of observation are usually inherent in graphical integration problems of this nature.

(6) An error of approximately one percent was obtained when comparing stress values obtained by Guyon with those calculated by the photoelastic method. A possible source of error could have been a result of the fringe pattern being altered slightly by the strain, in the CR 39, produced by the load on such a small model. The factor "K" was used to convert the maximum transverse tensile stress, obtained by the photoelastic method, to the maximum transverse tensile stress as found by Guyon.

The author makes the following recommendations:

(1) When designing a prestressed concrete end block it will be to the designer's advantage to spread the prestressing force over as large an area as possible. The length of the lead-in zone will be decreased as well as the steel requirements.

(2) The design procedures used in the analysis of end blocks are not exact but vary for each type loading arrangement. Therefore it is not possible to formulate an exact code for the design of end blocks. Experience and good judgment, on the part of the designer and the engineer in designing and placing the reinforcement, is required in order to obtain the desired structural behavior of a member.

BIBLIOGRAPHY

1. Preston, H. K. (1960) Practical Prestressed Concrete. McGraw-Hill Book Company, Inc. p. 1.

2. LIBBY, J. R. (1961) Prestressed Concrete Design and Construction. The Ronald Press Company, p. 405.

3. EVANS. R. H. & BENNETT, E. W. (1958) Prestressed Concrete Chapman & Hall Ltd., p. 92.

4. GUYON, Y. (1960) Prestressed Concrete. John Wiley and Sons, Inc. p. 127.

5. POPOV, E. P. (1952) Mechanics of Materials. Prentice-Hall, Inc. p. 42.

6. MORICE, P. B. & COOLEY, E. H. (1958) Prestressed Concrete. Sir Isaac Pitman & Sons, Ltd. p. 282.

7. MAGNEL, G. (1954) Prestressed Concrete. McGraw-Hill Company.

8. MOODY, W. T. & PHILLIPS, H. B. (1955) Photoelastic and Experimental Analog Procedures. United States Department of the Interior, Bureau of Reclamation. p. 1.

9. ZANDMAN, F. DR. (1959) Photostress, Principles and Applications. p. 1.

10. FROCHT, M. M. (1941) Photoelasticity. John Wiley and Sons, Inc.

11. TIMOSHENKO & GOODIER, (1951) Theory of Elasticity. McGraw-Hill Book Company, p. 87.

12. M. HETENYI, (1954) Handbook of Experimental Stress Analysis. John Wiley and Sons, p. 880.

VITA

Charles R. Hoffman was born on September 24, 1936 at Springfield, Missouri, the son of Mr. and Mrs. Raymond Hoffman.

Upon graduation from Central High School at Springfield, Missouri in 1954, he enrolled at the Missouri School of Mines and Metallurgy, Rolla, Missouri where he graduated in 1958.

He was employed by the Missouri State Highway Department at Springfield, Missouri, upon graduation for a period of seven months.

He was married to Miss Charlotte Ann Callaway of Springfield, Missouri in January, 1959.

In January 1959, he entered the United States Corps of Engineers for two years of active duty.

Upon release from active duty January 1961, he accepted a graduate assistantship in Civil Engineering at the Missouri School of Mines and Metallurgy and has served in that capacity to date.